Fractional Ca^{2+} currents through somatic and dendritic glutamate receptor channels of rat hippocampal CA1 pyramidal neurones

Olga Garaschuk, Ralf Schneggenburger, Claudia Schirra, Filippo Tempia and Arthur Konnerth*

Physiologisches Institut, Universität des Saarlandes, 66421 Homburg, Germany

1. The Ca^{2+} permeability of non-NMDA and NMDA receptor channels was studied using a fluorometric flux measurement approach in somata and dendrites of CA1 pyramidal neurones in rat hippocampal slices. For this purpose, the Ca^{2+} fraction of the total cation current (named 'fractional Ca^{2+} current') was measured directly from the change in the Ca^{2+}-sensitive fura-2 fluorescence at 380 nm excitation wavelength.

2. The fractional Ca^{2+} current through the somatic NMDA receptor channels was $10{\cdot}69 \pm 2{\cdot}13\%$ (mean ± S.D.) and that through dendritic receptor channels was $10{\cdot}70 \pm 1{\cdot}96\%$. The fractional Ca^{2+} current was not dependent on the extracellular Mg^{2+} concentration and its voltage dependence was in agreement with the Goldman–Hodgkin–Katz current equation.

3. AMPA (α-amino-3-hydroxy-5-methylisoxazole-4-propionate) or kainate applications produced small but significant Ca^{2+} entry. Fractional Ca^{2+} currents of $0{\cdot}58 \pm 0{\cdot}34\%$ were measured for somatic AMPA applications, $0{\cdot}68 \pm 0{\cdot}20\%$ for somatic kainate applications, $0{\cdot}66 \pm 0{\cdot}25\%$ for dendritic AMPA applications and $0{\cdot}61 \pm 0{\cdot}16\%$ for dendritic kainate applications.

4. The expression pattern of glutamate receptor subunits encoding messenger ribonucleic acids (mRNAs) was analysed with the single-cell reverse transcriptase-polymerase chain reaction (RT-PCR) approach applied to CA1 pyramidal neurones. The AMPA receptor subunits GluR-A, GluR-B and GluR-C, and the NMDA receptor subunits NR2A and NR2B were found to be abundantly expressed in all CA1 pyramidal neurones tested.

5. This study establishes the fractional Ca^{2+} current through somatic and dendritic NMDA and non-NMDA receptor channels in CA1 pyramidal neurones. The dendritic, presumably synaptic, NMDA receptor channels are highly Ca^{2+} permeable and have a fractional Ca^{2+} current closely resembling that of somatic extrasynaptic NMDA receptor channels. Both somatic and dendritic non-NMDA receptor channels are of the 'low Ca^{2+} permeable' type and have a fractional Ca^{2+} current that is about twenty times smaller than that of NMDA receptor channels.

The glutamate receptor channels play a key role in brain function. Most of the fast excitatory synaptic transmission in the central nervous system is mediated by glutamate receptor channels (for review Wisden & Seeburg, 1993; Hollmann & Heinemann, 1994). Besides this role, glutamate receptors have also been implicated in phenomena such as learning and memory, cellular differentiation and degeneration. On the basis of their pharmacological properties glutamate receptor channels have been classified into three major subtypes that are α-amino-3-hydroxy-5-methyl-4-isoxazole propionic acid (AMPA), kainate (KA) and *N*-methyl-D-aspartate (NMDA) receptors. Under physiological conditions fast excitatory synaptic transmission is mediated predominantly through AMPA and, probably, kainate receptor subtypes. At most synapses NMDA receptor activation becomes apparent only during high-frequency discharges that are able to evoke different forms of synaptic plasticity.

* To whom correspondence should be addressed.

Glutamate receptor channels are permeable to monovalent and, to some extent, divalent cations. While NMDA receptor channels were for a long time known to be highly permeable for Ca^{2+} ions, non-NMDA receptor channels were thought to have a very low Ca^{2+} permeability (Mayer & Westbrook, 1987). NMDA receptor-mediated Ca^{2+} entry was shown to be involved in many cellular functions including long-term potentiation (LTP) as well as glutamate-mediated neurotoxicity (Bliss & Collingridge, 1993; Lipton, 1993; Malenka & Nicoll, 1993). Recently, however, Ca^{2+} entry via AMPA/KA receptors has been demonstrated in several types of brain cell (Iino, Ozawa & Tsuzuki, 1990; Schneggenburger, Zhou, Konnerth & Neher, 1993; Jonas, Racca, Sakmann, Seeburg & Monyer, 1994).

Molecular biological studies have demonstrated that functional AMPA receptors may be obtained by various combinations of four different subunits: GluR-A, GluR-B, GluR-C and GluR-D (for review Hollmann & Heinemann, 1994). Expression of these subunits in different heterologous expression systems has demonstrated that Ca^{2+} can indeed permeate through either homomeric or heteromeric AMPA receptor channels whenever the receptor complex lacks the edited form of GluR-B subunit (Burnashev, Monyer, Seeburg & Sakmann, 1992; Keller, Hollmann, Heinemann & Konnerth, 1992). It has been suggested (Sommer, Köhler, Sprengel & Seeburg, 1991) that the Ca^{2+} permeability of the GluR-B subunit and, consequently, the Ca^{2+} permeability of the resulting homomeric or heteromeric receptor channel is determined by mRNA editing. A single amino acid residue in the second transmembrane domain (TMII, but see Hollmann, Maron & Heinemann, 1994) of the GluR-B subunits governs electrophysiological properties and also Ca^{2+} permeability of AMPA receptor channels (Hume, Dingledine & Heinemann, 1991).

This well-established body of knowledge regarding recombinant glutamate receptors contrasts with what is known about the Ca^{2+} permeability of fully differentiated, cell-specific neuronal receptors that are expressed *in vivo* in different regions of brain. Recent evidence suggested that the high Ca^{2+} permeability of AMPA receptors found in cultured hippocampal cells (Iino *et al.* 1990; Bochet *et al.* 1994) and neocortical interneurones (Jonas *et al.* 1994) is also caused by the lack of the edited form of the GluR-B subunit.

Moreover in large forebrain neurones of the medial septum (Schneggenburger *et al.* 1993) the fraction of Ca^{2+} ions in the net cation current through AMPA receptor channels was also shown to be rather high (on average 1·4%) and not negligible in comparison with the fraction of Ca^{2+} ions through NMDA receptor channels (on average 6·8%) in the same type of neurones. Here we use the same experimental approach (Schneggenburger *et al.* 1993) to obtain an estimation of the fractional Ca^{2+} current (P_f) through glutamate receptor channels of CA1 pyramidal neurones in hippocampal slices. We adapted this approach for measurements in cells with an extended dendritic tree. We found that in hippocampal pyramidal neurones the fractional Ca^{2+} current through non-NMDA receptor channels is rather low (P_f around 0·6%) while the Ca^{2+} permeability of NMDA receptor channels (P_f around 11%) is higher than in the medial septum. Further, our results demonstrate that there is a close similarity between somatic and dendritic glutamate receptor channels in terms of their Ca^{2+} permeability. To understand the molecular basis of the fractional Ca^{2+} currents we also performed single-cell RT-PCR analyses of the cellular mRNAs encoding different glutamate receptor subunits in CA1 hippocampal pyramidal neurones.

METHODS

Slice preparation and solutions

Hippocampal slices of 200 μm thickness were prepared from brains of young (8- to 17-day-old) Wistar rats as described previously (Edwards, Konnerth, Sakmann & Takahashi, 1989). Briefly, rats were decapitated by cervical dislocation and brain hemispheres were rapidly isolated and placed in an ice-cold bicarbonate-buffered standard saline (for composition see below). Slices were transferred to a storage chamber containing standard saline bubbled with a mixture of 95% O_2–5% CO_2. The temperature in the chamber was 34 °C for the first 30–60 min and was subsequently lowered to room temperature (22–24 °C).

The composition of the standard perfusion saline was (mM): 125 NaCl, 2·5 KCl, 2 $CaCl_2$, 1 $MgCl_2$, 1·25 NaH_2PO_4, 26 $NaHCO_3$ and 20 glucose (pH 7·4 when bubbled continuously with 95% O_2–5% CO_2). In most experiments, when NMDA receptor-mediated currents were studied, Mg^{2+} was omitted from the standard saline. To block voltage-gated sodium channels and postsynaptic currents mediated by γ-aminobutyric acid (GABA), 0·5 μM tetrodotoxin (TTX) and 20 μM bicuculline were added to the standard saline in all experiments. The standard pipette solution (intracellular solution) contained (mM): 130 CsCl, 20 tetraethylammonium chloride (TEACl), 4 Mg-ATP, 0·2 Na-GTP, 1 fura-2 penta-potassium salt and 10 Hepes (pH 7·3, adjusted with CsOH) when not otherwise stated. When measuring voltage-gated Ca^{2+} currents (see below), 20 mM TEACl was added also to the external saline to provide a better block of voltage-gated potassium channels.

All chemicals were purchased from Sigma, except for L-AMPA (Tocris, Essex, UK). The voltage-gated Ca^{2+}-channel blocker D-600 (gallopamil) was a gift from Knoll (Ludwigshafen, Germany).

Electrophysiological recordings and drug application

Experiments were performed at room temperature in set-ups equipped with upright microscopes (Axioscope FS, Zeiss; for details see also Eilers, Schneggenburger & Konnerth, 1995). Before establishing the whole-cell recording configuration, CA1 pyramidal neurones were visually identified and their membrane surface 'cleaned' using the procedures described previously (Edwards *et al.* 1989). Patch pipettes made of borosilicate glass (Hilgenberg, Germany), with resistances of 2–3 MΩ when filled with the intracellular solution, were coated with Sylgard resin (General Electrics, Ruesselsheim, Germany). Ionic currents were

recorded with the EPC-9 patch-clamp amplifier (HEKA, Lambrecht, Germany). The holding potential was set, when not otherwise indicated, at −60 mV. Data acquisition and pulse protocols for controlling the agonist application (see below) were performed using the Pulse software (HEKA). Recordings were accepted for later analysis if the series resistance did not exceed 10–12 MΩ even during extended periods of whole-cell recording (up to 40–50 min). The series resistance was always compensated (up to 60%) following standard procedures.

Glutamate receptor agonists were applied from an ionophoresis pipette filled with agonist solution (10 mM of AMPA, kainate or NMDA, respectively, each buffered with 10 mM Hepes, pH 7·4). Ejection currents of −1 μA with variable durations of 30–500 ms were applied using an ionophoresis system (NPI Electronic, Tamm, Germany). Positive retaining currents in the range +20 to +40 nA were applied between agonist applications to avoid leak of the agonist. Ca^{2+} entry through voltage-gated Ca^{2+} channels was completely blocked by using D-600 at a concentration of 500 μM in all experiments in which the fractional Ca^{2+} current through ligand-gated channels was measured. The completeness of this block was reached within about 10 min of perfusion with 500 μm D-600 and was routinely confirmed by applying depolarizing pulses (from −60 to 0 mV for 2 s) prior to agonist application experiments.

Fluorometric Ca^{2+} measurements

Fluorometric Ca^{2+} measurements were performed with fura-2 (pentapotassium salt, Molecular Probes), which was added to the intracellular solution at a concentration of 1 mM (sometimes 2 mM) and loaded into the cell via the patch pipette. The measurements using a photomultiplier system (Luigs and Neumann, Ratingen, Germany) were similar to those described in Schneggenburger *et al.* (1993). Briefly, the fluorescence, produced by alternating excitation light of 360 and 380 nm wavelength at a frequency of 4 Hz, was collected from a circular area of 50 μm, into which the soma of a CA1 neurone was placed. The fluorescence signals were sampled at 2 Hz, and thus represented spatial and temporal averages. The intracellular free Ca^{2+} concentration ($[Ca^{2+}]_i$) was calculated from the fluorescence ratio according to Grynkiewicz *et al.* (1985). The calibration constants K_{eff} (effective binding constant), R_{min} (fluorescence ratio at zero Ca^{2+}) and R_{max} (limiting fluorescence ratio at high Ca^{2+}) were obtained from '*in vivo*' calibration experiments (Neher, 1989; Eilers *et al.* 1995). Typical calibration parameters found for K_{eff}, R_{min} and R_{max} in this particular set-up were 1006 nM, 0·53, and 4·86, respectively.

In the experiments in which somatic and dendritic fluorescence changes were monitored simultaneously we used a slow-scan digital imaging system (T.I.L.L. Photonics GmbH, München, Germany) with Image-8 software (University of Saarland, Homburg, Germany). Background images of the preparation were obtained in the cell-attached mode for each ultraviolet (UV) excitation wavelength (360 nm for the isosbestic and 380 nm for the Ca^{2+}-sensitive wavelength, respectively). Following the establishment of the whole-cell configuration, the loading of the cell with fura-2 was monitored as a gradual increase in the Ca^{2+}-independent fluorescence signal. Measurements were started only after equilibration of the fura-2 concentration between pipette and all cellular compartments of interest (e.g. soma and dendrites) as indicated by stable maximal intensity signals at 360 nm excitation wavelength. In general, the time taken to reach this equilibrium was about 10 min.

Routinely, fluorescence values representing spatial averages from defined pixel regions were transferred on-line through a serial port to another personal computer and displayed there as a function of time together with the whole-cell current recording (Eilers *et al.* 1995). The background fluorescence was measured in a separate pixel region near the cell and used for an on-line correction of the cellular fluorescence signals. Typical values measured for K_{eff}, R_{min} and R_{max} in the imaging set-up were 1048 nM, 0·67 and 4·2, respectively. In some instances, consecutive paired exposures to 360 and 380 nm were used to construct background-corrected digital fluorescence images. They were displayed on-line in a pseudocolour mode on a monitor and stored on hard disk for later analysis.

To enable a comparison of the Ca^{2+}-sensitive fluorescence signals between the two different set-ups and between data presented in this paper and data acquired by other laboratories, the arbitrary fluorescence values were normalized by the fluorescence value of standard fluorescent beads (4·5 μm diameter; Polysciences Inc., Warrington, PA, USA). In the photomultiplier-based set-up, one bead at a time was placed in the measuring area, and the fluorescence value was taken at 380 nm excitation wavelength. In the imaging system, a square pixel region of sufficiently large dimension (about 10 × 10 μm) was defined around a bead to measure the spatially averaged bead fluorescence. The cellular fluorescence values at 380 nm excitation wavelength (F_{380}) were divided by the average ($n = 5$) bead fluorescence determined under the same recording conditions. The resulting fluorescence unit was termed 1 bead unit (BU) (Zhou & Neher, 1993; Schneggenburger *et al.* 1993).

Estimation of the fractional Ca^{2+} current

The measured change in Ca^{2+}-sensitive fura-2 fluorescence (ΔF_{380}) was related to the net cation current according to the following equation (Neher & Augustine, 1992):

$$f = \Delta F_{380} \int I \, dt, \quad (1)$$

in which f is also called the F/Q ratio (the ratio of the decrement in the fluorescence F over the current integral Q) and is measured in bead units per electrical charge and $\int I \, dt$ is the integral over time of the net cation current. The F/Q ratio was determined for a rather brief time interval as explained in Schneggenburger *et al.* (1993). The percentage of Ca^{2+} contributing to the net cation charge (called fractional Ca^{2+} current or P_f; Schneggenburger *et al.* 1993) was then obtained by dividing the F/Q ratio by a constant which gives ΔF_{380} per unit of pure Ca^{2+} charge. This constant was termed f_{max}. For the analysis of the smaller dendritic responses, we preferred to determine F/Q ratios by a second, more accurate approach involving a fitting of the measured F_{380} signals with baseline-corrected time integrals of the agonist-activated currents (see Figs. 2*A*, 5 and 9), assuming a single rate constant calcium extrusion mechanism (eqn (8) in Schneggenburger *et al.* 1993).

The f_{max} value can be obtained by relating ΔF_{380} to the entering Ca^{2+} charge measured as the time integral of the whole-cell current due to the opening of highly Ca^{2+}-selective ion channels. Several series of experiments were performed to determine the f_{max} value in CA1 pyramidal neurones. Voltage-gated Ca^{2+} currents were recorded with intracellular and extracellular solutions (see above) designed to isolate the Ca^{2+} current component. In the first series of experiments, the photomultiplier was used to collect changes in the Ca^{2+}-dependent fura-2 fluorescence ΔF_{380} over a circular area of 50 μm (corresponding to the soma, parts of the basal dendrites

and a short segment of the apical dendrite, see Fig. 1*A*). The value of f_{max} under these conditions was 9·05 ± 0·53 BU nC^{-1} ($n = 5$ cells). A similar series of experiments was performed using the slow-scan digital imaging system (see above) in order to also collect the fluorescence changes originating from the more distal parts of the dendritic tree. Under these conditions an f_{max} value of 8·79 ± 1·89 BU nC^{-1} ($n = 4$ cells) was determined. In a third series of experiments, the apical dendrite of a CA1 neurone was cut off with a fine pipette prior to whole-cell recording. The value of f_{max} determined under these conditions using the imaging system was 8·84 ± 0·09 BU nC^{-1} ($n = 3$ cells). The three sets of values were pooled to give a common average value of f_{max} (8·82 ± 0·47 BU nC^{-1}, $n = 12$ cells), which was used to calculate the fractional Ca^{2+} currents from the experimentally obtained F/Q ratios for AMPA- and NMDA-activated currents.

Simulation of constant field behaviour

To obtain a prediction of P_f at different membrane potentials, we consider predictions of the Goldman–Hodgkin–Katz (GHK) current equation. The current carried by an ionic species of valency z_i is given by:

$$I_i = \frac{Fz_i^2 P_i \psi (C_{i,o} - C_{i,i}\exp(\psi z_i))}{1 - \exp(\psi z_i)}, \quad (2)$$

where $\psi = VF/RT$, V is membrane potential, F, R and T are standard thermodynamic parameters, C is concentration of ion i inside or outside the cell (subscript i or o, respectively) and P is absolute GHK permeability of ion i. We assume that Ca^{2+} has a permeability P_{Ca} and is present outside at a concentration $[Ca^{2+}]_o$ and inside at a concentration $[Ca^{2+}]_i$. Then

$$I_{Ca} = \frac{4FP_{Ca}\psi([Ca^{2+}]_o - [Ca^{2+}]_i\exp(2\psi))}{1 - \exp(2\psi)}. \quad (3)$$

Assuming that monovalents have the lumped permeability P_M and are present outside at a concentration $[M]_o$ and inside at a concentration $[M]_i$ we obtained:

$$I_M = \frac{FP_M\psi([M]_o - [M]_i\exp\psi)}{1 - \exp\psi} \quad (4)$$

and, therefore,

$$P_f = \frac{I_{Ca}}{I_{Ca} + I_M}$$

$$= \frac{4[Ca^{2+}]_o(1 - \exp\psi)}{4[Ca^{2+}]_o(1-\exp\psi) + P_M/P_{Ca}(1-\exp(2\psi))([M]_o - [M]_i\exp\psi)}. \quad (5)$$

This equation was obtained assuming that $[Ca^{2+}]_i$ is negligible. $[Ca^{2+}]_o$, the extracellular free Ca^{2+} concentration, was determined to be 1·6 mM (Schneggenburger *et al.* 1993). Further, assuming that the monovalents that are present inside and outside have an equal total concentration [M], eqn (5) becomes:

$$P_f = \frac{4[Ca^{2+}]_o}{4[Ca^{2+}]_o + P_M/P_{Ca}[M](1 - \exp(2\psi))}. \quad (6)$$

This equation is identical to the equation (7) in Schneggenburger *et al.* (1993), but note that in the original equation the '1' is missing in '1 − exp(2ψ)'. To obtain a non-linear least-square fit of this equation to the experimental data the ratio of monovalent over divalent permeability (P_M/P_{Ca}) was varied as the free parameter.

Single-cell RT-PCR analysis of AMPA and NMDA receptor subunits

For the single-cell RT-PCR (reverse transcriptase-polymerase chain reaction) analysis, the content of a CA1 pyramidal neurone was harvested via the pipette (tip opening around 10 μm) by applying negative pressure for 5–10 min in the presence of a vanadyl–ribonucleoside complex (Gibco-BRL), to inhibit RNAase activity. The pipette was filled with 8 μl of an autoclaved solution containing (mM): 140 CsCl, 3 $MgCl_2$, 5 EGTA, 10 Hepes (pH 7·2). To avoid contamination with mRNAs from other cells, the diameter of the pipette was chosen to be smaller than the diameter of the cell so that tight contact between the cell and the pipette was maintained during the process of harvesting. The process of aspiration was visually controlled using an upright microscope (Axioscope FS). After being harvested, the content of the cell was expelled into a PCR tube where the reverse transcriptase (RT) reaction was performed (for details see Lambolez, Audinat, Bochet, Crepel & Rossier, 1992).

Products of the RT reaction were divided in two parts. One part was amplified with primers common for all AMPA receptor subunits (GluR-A and GluR-D; the same primers as in Lambolez *et al.* 1992), the other part was amplified with primers common for NMDA receptor subunits (NR2A–NR2C; the same primers as in Audinant, Lambolez, Rossier & Crepel, 1994). The polymerase chain reaction (PCR) was performed with a programmable thermocycler (Biometra, Göttingen, Germany) under the conditions described in Lambolez *et al.* (1992) for AMPA receptor subunits and under the conditions described in Audinant *et al.* (1994) for NMDA receptor subunits. The product of the first PCR was isolated from a preparative agarose (Gibco-BRL) gel and reamplified with the same set of primers. The product of the second PCR was analysed by subunit-specific restriction enzymes. The four enzymes, *Bg*II, *Eco*47III, *Eco*RI (all purchased from Stratagene GmbH, Heidelberg, Germany) and *Bsp*1286I (Serva, Heidelberg, Germany), selectively cut the GluR-A, GluR-C, GluR-D and GluR-B PCR fragments. Three enzymes, *Bpm*I, *Bfa*I (purchased from New England Biolabs, Beverly, MA, USA) and *Sca*I (purchased from Pharmacia, Freiburg, Germany), were chosen to cut selectively the NR2A, NR2B and NR2C PCR fragments. The restriction reaction was then analysed by agarose gel electrophoresis.

Data are given as means ± S.D. unless otherwise stated.

RESULTS

Measurement of the Ca^{2+} influx through NMDA receptor channels in hippocampal CA1 pyramidal cells

To measure the NMDA receptor-mediated Ca^{2+} influx and the corresponding fractional Ca^{2+} currents we used an approach that was similar to that described previously by Schneggenburger *et al.* (1993) for medial septal neurones. Figure 1*A* illustrates schematically the experimental arrangement in which whole-cell recordings were combined with fluorometric measurements. The strict localization of the postsynaptic responses evoked with local ionophoretic agonist application was confirmed by fluorometric imaging experiments (see Figs 5 and 6). Figure 1*B* shows that after

establishing the whole-cell recording mode fura-2 starts to diffuse from the patch pipette into the cell. The fluorescence at the Ca^{2+}-insensitive wavelength F_{360} (Fig. 1*Ba*) represents a direct measure of the intracellular fura-2 concentration and was calibrated accordingly. Shortly after the beginning of the whole-cell recording, NMDA was repeatedly applied to the soma causing brief inward current responses (Fig. 1*Bd*) and corresponding increases in free intracellular Ca^{2+} concentration (Fig. 1*Bc*). While the amplitudes of the transient increases in $[Ca^{2+}]_i$ gradually decreased (Fig. 1*Bc*), the amplitudes of the Ca^{2+}-sensitive fluorescence decrements (ΔF_{380}; Fig. 1*Bb*) increased with the increase in intracellular fura-2 concentration. Thus, as has been previously shown for Ca^{2+} entry through voltage-gated channels (Neher & Augustine, 1992; Schneggenburger *et al.* 1993), fura-2 eventually overrides the endogenous buffers and almost all Ca^{2+} ions entering through NMDA receptor channels are captured by fura-2 (see also Fig. 2*B*). In these recording conditions, the decrements in fluorescence ΔF_{380} are proportional to the Ca^{2+} charge entering the cell through the NMDA channels (Q_{NMDA}) (Fig. 2*A*, for details see Methods). For the NMDA application shown on Fig. 2*A* an f_{NMDA} value of 0·957 was obtained by dividing ΔF_{380} over Q_{NMDA} at 1·7 s after the initiation of the NMDA-mediated current and an f_{NMDA} value of 0·962 was obtained using the curve-fitting approach (see Methods).

In Fig. 2*B*, the ratios of ΔF_{380} over the NMDA-mediated current integral, named f_{NMDA} (see eqn (1)), of all NMDA-mediated responses recorded during the experiment shown in Fig. 1*B* were plotted as a function of the Ca^{2+}-binding capacity of fura-2 (κ'_B). κ'_B was calculated according to the equation

$$\kappa'_B = \frac{[B]/K_D}{(1+[Ca^{2+}]_{i,a}/K_D)(1+[Ca^{2+}]_{i,b}/K_D)}, \quad (7)$$

where $[Ca^{2+}]_{i,b}$ and $[Ca^{2+}]_{i,a}$ are values of $[Ca^{2+}]_i$ before and after agonist application, respectively, K_D is the dissociation constant of fura-2 and [B] is the total intracellular concentration of fura-2 (see also Neher & Augustine, 1992).

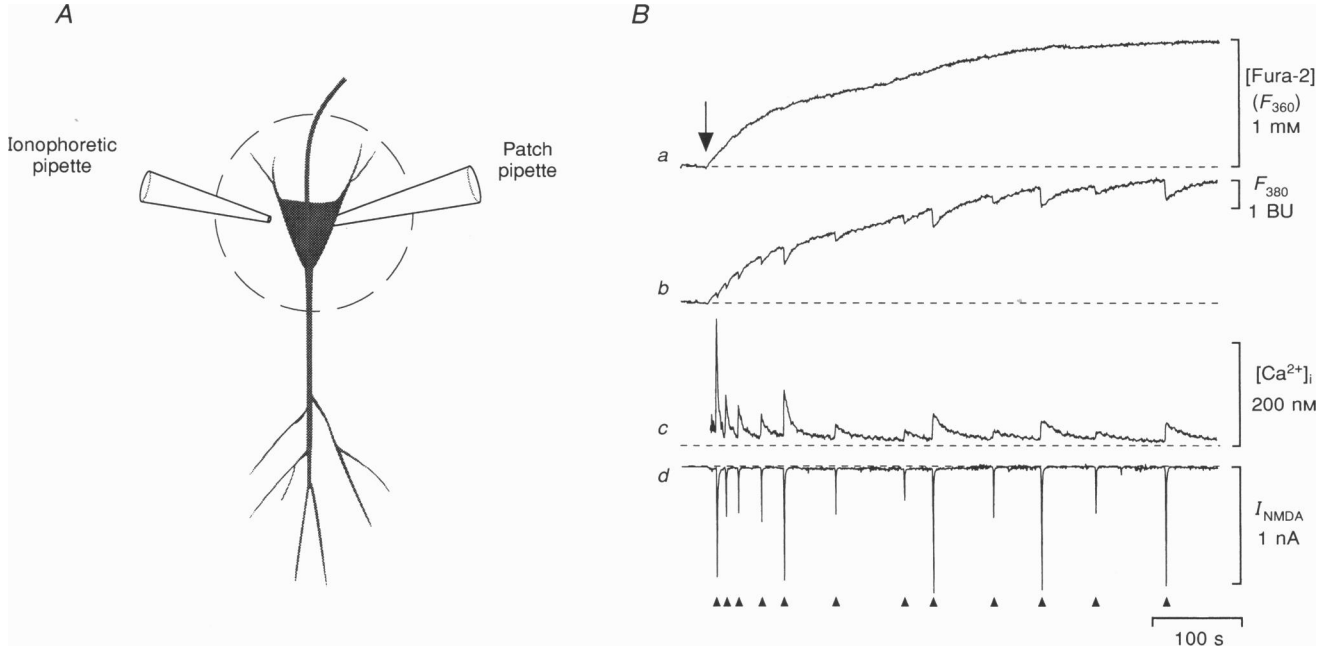

Figure 1. Measurement of the Ca^{2+} influx through NMDA receptor channels in a hippocampal CA1 pyramidal cell

A, scheme of the experimental arrangement. The light-sensitive area of the photomultiplier (50 μm diameter) is depicted as a circle and shows the part of the neurone in which the fura-2-mediated fluorometric changes shown in *B* were recorded. *B*, traces represent: *a*, fluorescence at 360 nm excitation wavelength (F_{360}); *b*, Ca^{2+}-sensitive fluorescence at 380 nm excitation wavelength (F_{380}); *c*, intracellular free Ca^{2+} concentration ($[Ca^{2+}]_i$); and *d*, whole-cell membrane current (I_{NMDA}). F_{360} is Ca^{2+} insensitive and was used to estimate the fura-2 concentration inside the cell. The arrow indicates the beginning of the whole-cell recording. Here and in the subsequent figures ionophoretic applications of NMDA were performed at time points marked with the arrowheads; fluorescence changes are given in bead units (BU) representing the fluorescence intensity of a fluorescent bead at 380 nm excitation wavelength (Zhou & Neher, 1993; Schneggenburger *et al.* 1993).

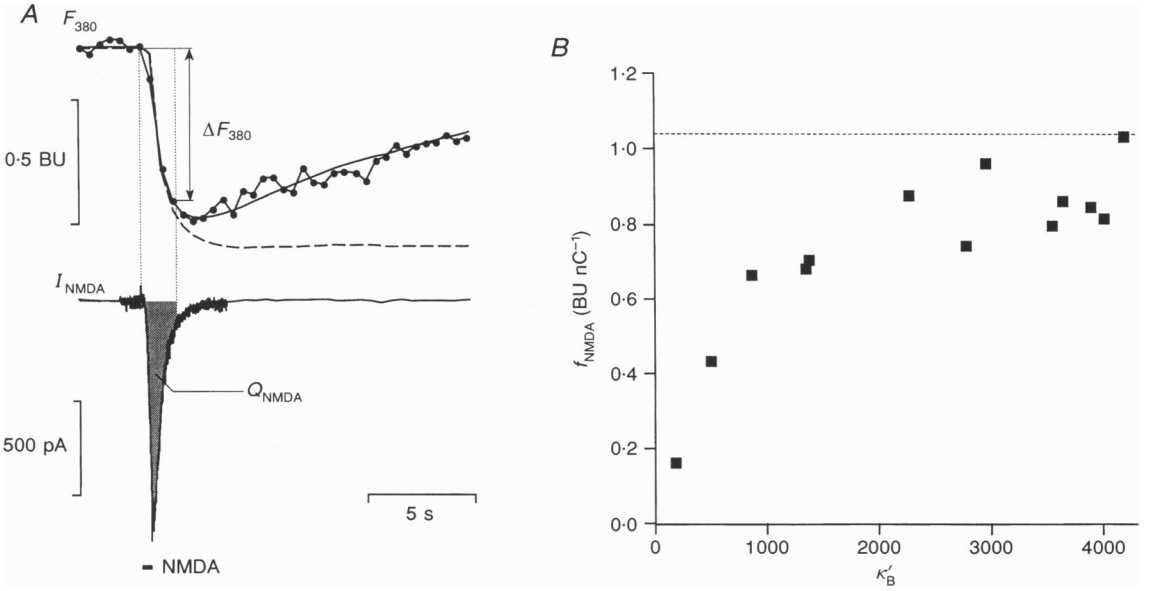

Figure 2. Determination of f_{NMDA} and its dependence on the Ca^{2+}-binding capacity of fura-2

A, NMDA-evoked whole-cell current (bottom) and the simultaneously recorded F_{380} trace (top). The corresponding F/Q ratio (or f_{NMDA}) can be determined by two procedures. First, by dividing the decrement in fluorescence (ΔF_{380}) by the charge which entered through the NMDA channels (Q_{NMDA}; shaded area). Second, the F_{380} trace was fitted (continuous line) with the scaled time integral (dashed line) of the underlying whole-cell current response I_{NMDA}. From this simulation, estimates of f_{NMDA} and the decay time constant of the fluorescence signal were obtained (see Methods). *B*, plot of f_{NMDA} as a function of the Ca^{2+}-binding capacity of fura-2 (κ'_B, see eqn (7)). Data points represent the result of the analyses of all NMDA applications during the experiment shown on Fig. 1*B*. The dashed horizontal line depicts the maximal value of f_{NMDA} that was obtained from the double reciprocal plot as an intercept with the ordinate.

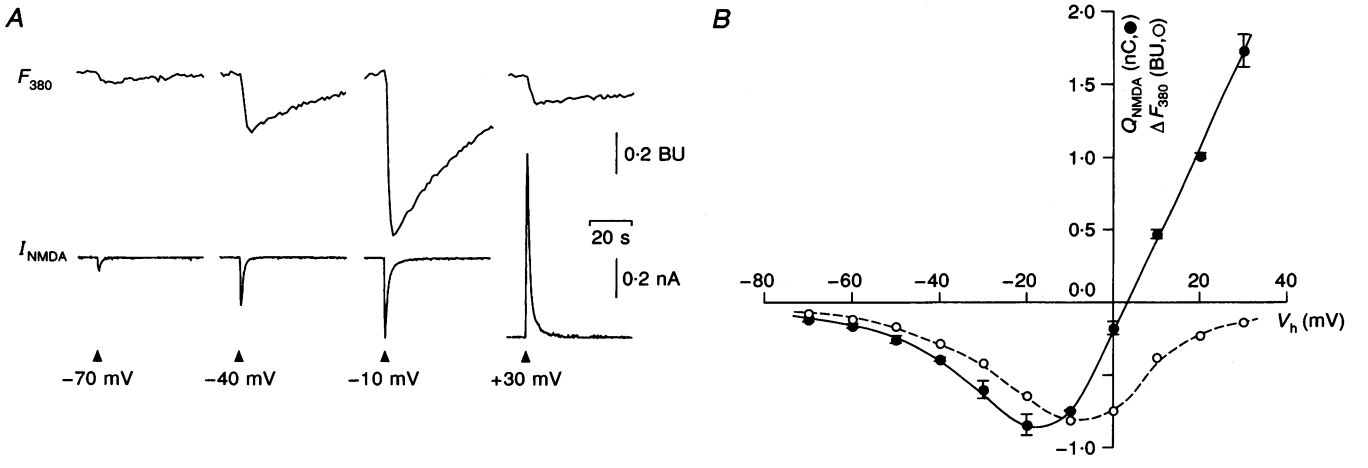

Figure 3. Voltage dependence of the Ca^{2+} flux through NMDA receptor channels

A, F_{380} traces and corresponding whole-cell currents owing to ionophoretic applications of NMDA (35 ms, 1 μA) at different holding potentials as indicated. Each trace is an average of $n = 4$ consecutive responses. *B*, Q_{NMDA}, calculated as the time integral of the NMDA-evoked currents, and the corresponding decrements in F_{380} (ΔF_{380}), plotted as a function of holding voltage (V_h). Error bars represent mean ± S.D. for 4 different applications at each holding potential. For ΔF_{380} recordings, the length of the error bars is less than the diameter of the symbols. Note that there is significant Ca^{2+} entry even at positive holding voltages (+ 10 to +30 mV) during NMDA-mediated net outward currents.

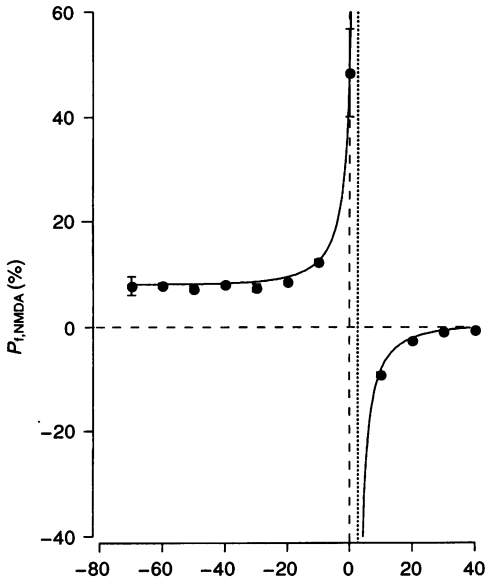

Figure 4. The Ca^{2+} fraction of the cation current through NMDA receptor channels is not dependent on the voltage-dependent Mg^{2+} block

Voltage dependence of $P_{f,NMDA}$ within the holding potential range −70 to 40 mV. The superimposed continuous lines represent the non-linear least-square fit of the data to eqn (5) (see Methods) with a P_{Ca}/P_M value of 2·067 ± 0·003 for this particular cell. The fit was done using an option provided by the data analysis program (Igor, Wave Metrics, Lake Oswego, OR, USA). The vertical dotted line was traced through the reversal potential value (+ 3·43 mV) predicted by eqn (5). Results from the experiment illustrated in Fig. 3.

The plot in Fig. 2*B* shows that with the increase in the Ca^{2+}-binding capacity of fura-2, f_{NMDA} values became larger and, finally, reached a saturating level. The dashed line indicates the maximal value of f_{NMDA} obtained from a double reciprocal plot ($1/f_{NMDA}$ *versus* $1/\kappa'_B$) as intercept of the linear fit with the *y*-axis (Neher & Augustine, 1992). For practical purposes, the maximal value of f_{NMDA} was determined by averaging the data points obtained at $\kappa'_B > 2000$ (this corresponds to an intracellular fura-2 concentration of more than 800 μM at a basal $[Ca^{2+}]_i \leqslant 45$ nM for this cell). By dividing the hereby obtained value of f_{NMDA} (0·88 ± 0·09 BU nC^{-1}) by f_{max}

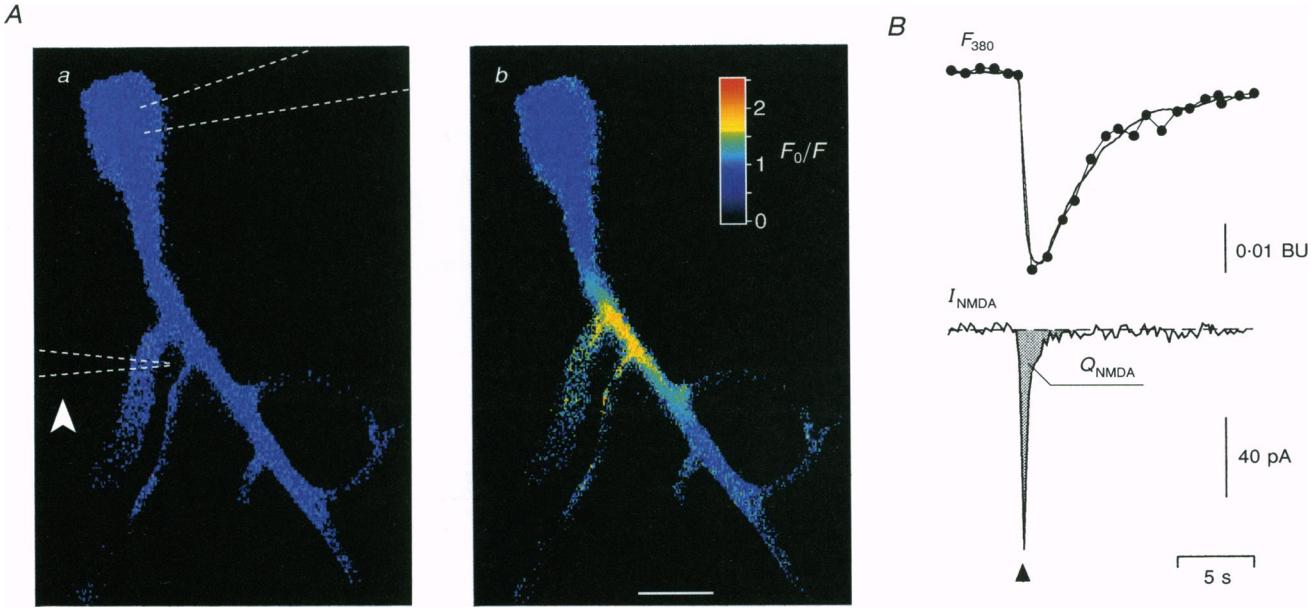

Figure 5. Measurement of Ca^{2+} fluxes through dendritic NMDA receptor channels

A, pseudocolour fluorescence images illustrating NMDA receptor-mediated Ca^{2+} changes in the dendritic region of a CA1 pyramidal neurone. Images taken before (*a*) and during (*b*) the ionophoretic NMDA application (50 ms, 1 μA). The positions of the ionophoresis (arrowhead) and the patch pipette are schematically indicated in image *a*. Scale bar in *a* and *b*, 20 μm. *B*, NMDA-evoked membrane current (bottom) and dendritic F_{380} trace (top) corresponding to the images shown in *A*. The shaded area corresponds to the total charge that entered through NMDA-activated channels (Q_{NMDA}). A simulation of the F_{380} trace (continuous line) was obtained as explained in the legend of Fig. 2 and is superimposed on the measured fluorescence signal.

(8·82 BU nC^{-1}; see also Methods), a fractional Ca^{2+} current of 9·98% was calculated for this particular cell. By analysing 302 NMDA-mediated responses in thirty-seven distinct CA1 hippocampal pyramidal neurones, we obtained a mean fractional Ca^{2+} current of 10·69 ± 2·13% through somatic NMDA receptor channels at a membrane potential of −60 mV and an extracellular Ca^{2+} concentration of 1·6 mM.

Voltage dependence of the Ca^{2+} influx through NMDA receptor channels

Figure 3*A* shows NMDA-mediated whole-cell currents and the simultaneously recorded F_{380} responses at four different holding potentials recorded in standard perfusion saline (1 mM Mg^{2+}). In Fig. 3*B* the time integrals of the current responses (Q_{NMDA}), representing the net charge crossing the membrane, and corresponding ΔF_{380} values were plotted as a function of membrane potential. Q_{NMDA} responses displayed the well-known voltage dependence reported previously to be due to the presence of extracellular Mg^{2+} ions (Nowak, Bregestovski, Ascher, Herbet & Prochiantz, 1984; Mayer & Westbrook, 1987). The Ca^{2+}-sensitive F_{380} decrements closely paralleled the net charge movements at membrane potentials between −70 and −20 mV. Remarkably, a significant Ca^{2+} inflow through NMDA-activated receptor channels was preserved even when the total cation charge crossing the membrane was negligible or even outward (voltage range from 0 to +30 mV). The maximal Ca^{2+}-dependent change in fluorescence was detected around −10 mV.

In Fig. 4 the fractional Ca^{2+} current ($P_{f,NMDA}$), calculated from the measured net ionic charges and the fura-2-detected ΔF_{380} signals, were plotted against the membrane potential. $P_{f,NMDA}$ was found to be nearly constant in the physiologically relevant voltage range between −70 and −20 mV. This indicates that the voltage-dependent relief from the Mg^{2+} block (Nowak *et al.* 1984; Mayer & Westbrook, 1987) affected similarly both the Ca^{2+} influx and the net charge transport through NMDA receptor channels. These results show that $P_{f,NMDA}$ is independent of the Mg^{2+} blockade of NMDA receptor channels (Schneggenburger *et al.* 1993; Burnashev, Zhou, Neher & Sakmann, 1995). The voltage dependence of the fractional Ca^{2+} current was in a first approximation in good agreement with the predictions of the Goldman–Hodgkin–Katz current equation, as is illustrated by the superimposed fit in Fig. 4 (see eqn (5)).

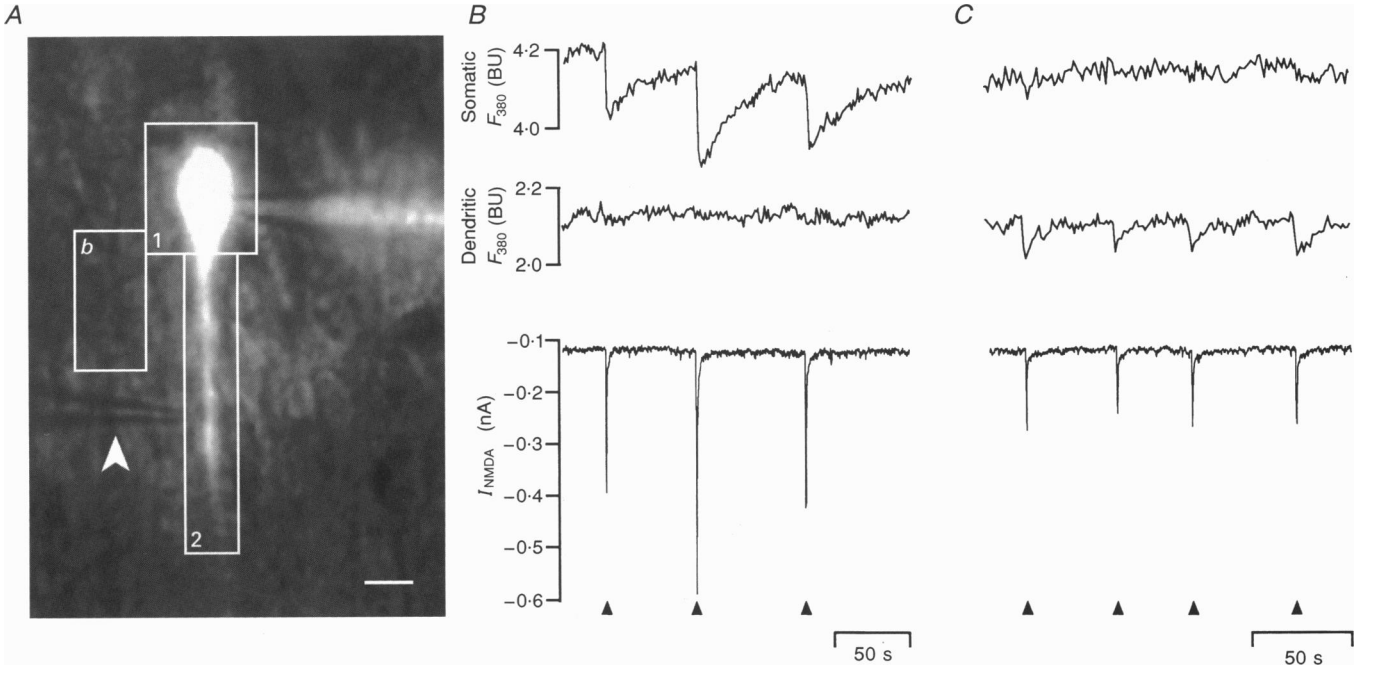

Figure 6. Comparison of local ionophoretic NMDA applications to soma and dendrites of the same cell

A, combined epifluorescence and transmitted light image of a CA1 pyramidal neurone in a hippocampal slice with a somatic patch pipette and a dendritic ionophoresis pipette (arrowhead). The background-corrected fluorescence signals shown in the top and middle traces of panels *B* and *C* were obtained from the somatic (1) and the dendritic (2) regions respectively. The mean auto fluorescence of the tissue was determined in the region of interest *b*. Scale bar, 20 μm. *B* and *C* show simultaneously recorded fluorescence (F_{380}) and whole-cell current (I_{NMDA}) signals in response to somatic (80–100 ms, 1 μA) and dendritic (30 ms, 1 μA) NMDA applications respectively. The image shown in panel *A* was taken during dendritic NMDA applications. Note the different time scales in *B* and *C*.

Ca^{2+} fluxes through dendritic NMDA receptor channels

Figure 5 illustrates an experiment designed to measure Ca^{2+} fluxes through dendritic NMDA receptor channels. By placing the ionophoresis pipette sufficiently close to the dendrites of interest and by applying NMDA for a short time (20–50 ms), Ca^{2+}-dependent changes in fluorescence were restricted to a relatively small region (Fig. 5*Ab*). Under these conditions it was possible to avoid significant activation of NMDA receptors located on dendrites that were not in the plane of focus. Figure 5*B* shows the F_{380} and the corresponding whole-cell current responses obtained from the activation of dendritic NMDA receptors. A notable difference between dendritic and somatic recordings was the shorter duration of the dendritic fluorescence signals. For similar whole-cell current responses of about 2–4 s duration the decay time constant of the F_{380} signals was in the range 15–20 s for somatic but in the range 3–6 s for dendritic NMDA applications (compare for example Fig. 5*B* with Fig. 2*A*). This difference is probably due to the difference in surface-to-volume ratio (J. Eilers, G. Callewaert, C. M. Armstrong & A. Konnerth, unpublished observations).

To obtain accurate estimates of $P_{f,NMDA}$ from the dendritic responses, F_{380} traces were fitted by the scaled integral of the corresponding whole-cell current (see Methods) rather than analysed by calculating the F/Q ratios. With this approach we obtained a decay time constant, t, of 3·1 s and an f_{NMDA} value of 0·87, yielding a $P_{f,NMDA}$ value of 9·86% for the dendritic NMDA-mediated response shown in Fig. 5*B*. By averaging the mean $P_{f,NMDA}$ values from nine neurones, a fractional Ca^{2+} current through dendritic NMDA receptor channels of 10·70 ± 1·96% was calculated.

In seven neurones the $P_{f,NMDA}$ value measured from a dendritic region was compared with the $P_{f,NMDA}$ value obtained from somatic recordings in the same cell. A representative experiment is illustrated in Fig. 6. In this

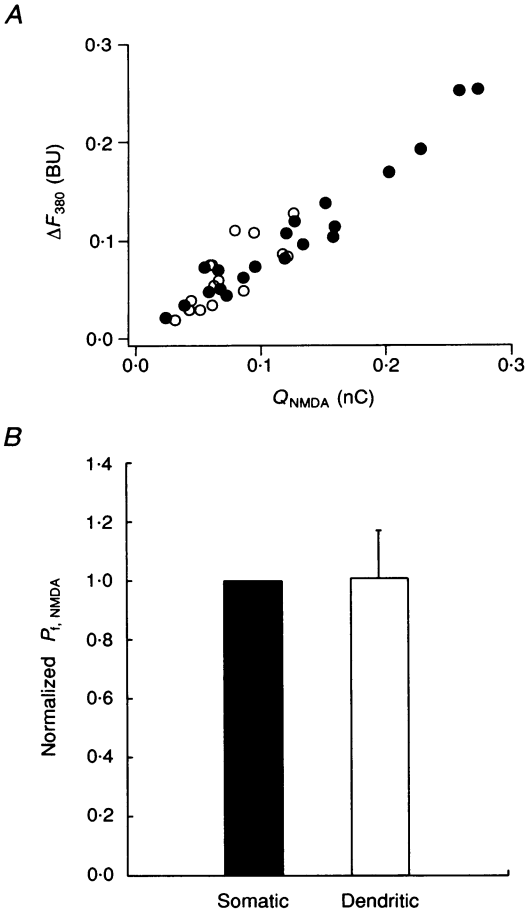

Figure 7. Comparison of fractional Ca^{2+} currents through somatic and dendritic NMDA receptor channels

A, plot of somatic (●, $n = 20$) and dendritic (○, $n = 17$) NMDA-mediated decrements in fluorescence, ΔF_{380}, against the corresponding charge Q_{NMDA}. Note that the proportionality between ΔF_{380} and Q_{NMDA} is constant over a wide range of amplitudes of these NMDA-mediated responses. *B*, comparison of somatic (■) and dendritic (□) $P_{f,NMDA}$ values that were obtained pairwise in $n = 7$ neurones. Each dendritic $P_{f,NMDA}$ value was normalized with respect to the corresponding somatic value yielding a mean of 1·01 ± 1·16.

experiment, after applying NMDA to the soma (Fig. 6*B*), the ionophoresis pipette was moved to a dendritic region (Fig. 6*C*). This procedure could be repeated several times yielding local responses confined specifically to the site of NMDA application. In general, smaller amounts of NMDA were applied to the dendrites yielding smaller responses (Fig. 6*C*) to minimize errors resulting from activation of NMDA receptors located on out of focus dendrites. With this precaution consistent results were obtained for all dendritic recordings. The validity of these measurements was confirmed by the graph in Fig. 7*A* showing that there is a direct proportionality between the ΔF_{380} values and the corresponding Q_{NMDA} responses. In addition, this analysis indicates that the $P_{f,NMDA}$ values obtained in soma and dendrites are highly similar. Indeed, when the somatic and dendritic F_{380} signals were analysed pairwise for each of these seven neurones, we obtained virtually identical $P_{f,NMDA}$ values (Fig. 7*B*).

No contamination of the fluorescence signals by Ca^{2+}-induced Ca^{2+} release

Under more physiological conditions, the activation of NMDA receptors was recently suggested to evoke Ca^{2+}-induced Ca^{2+} release (CICR) from the internal stores in CA1 hippocampal pyramidal neurones (Alford, Frenguelli, Schofield & Collingridge, 1993). If CICR contributed to the Ca^{2+} flux measurements in our experimental conditions, it would lead to an overestimation of fractional Ca^{2+} currents through the NMDA receptor channels. To examine this possibility, a series of experiments was performed in which Ruthenium Red, known to eliminate CICR and caffeine-mediated Ca^{2+} signals in central neurones (Kano, Garaschuk, Verkhratsky & Konnerth, 1995) was added to the pipette solution.

In our experimental conditions (when dialysing the cells with 1 mM fura-2) bath application of 20 mM caffeine produced F_{380} changes reflecting Ca^{2+} release from the internal stores (Fig. 8*A*, upper panel). The caffeine-mediated F_{380} signals were virtually completely blocked when CA1 neurones were internally perfused with 20 μM Ruthenium Red (Fig. 8*A*, lower panel). On average, internal Ruthenium Red reduced the caffeine-induced Ca^{2+} signals by 97% (see histogram in Fig. 8*B*), demonstrating that 20 μM Ruthenium Red effectively blocked caffeine-induced Ca^{2+} release in these experimental conditions. When fractional Ca^{2+} currents through somatic NMDA receptor channels were measured in the presence of 20 μM Ruthenium Red ($10{\cdot}87 \pm 2{\cdot}14\%$, $n = 6$ cells), no significant difference from the value of the control group was found suggesting that CICR did not contaminate the measurements of fractional Ca^{2+} currents.

Fractional Ca^{2+} currents through somatic and dendritic non-NMDA receptor channels

Figure 9 shows whole-cell currents and the corresponding fluorescence changes in response to kainate applications to

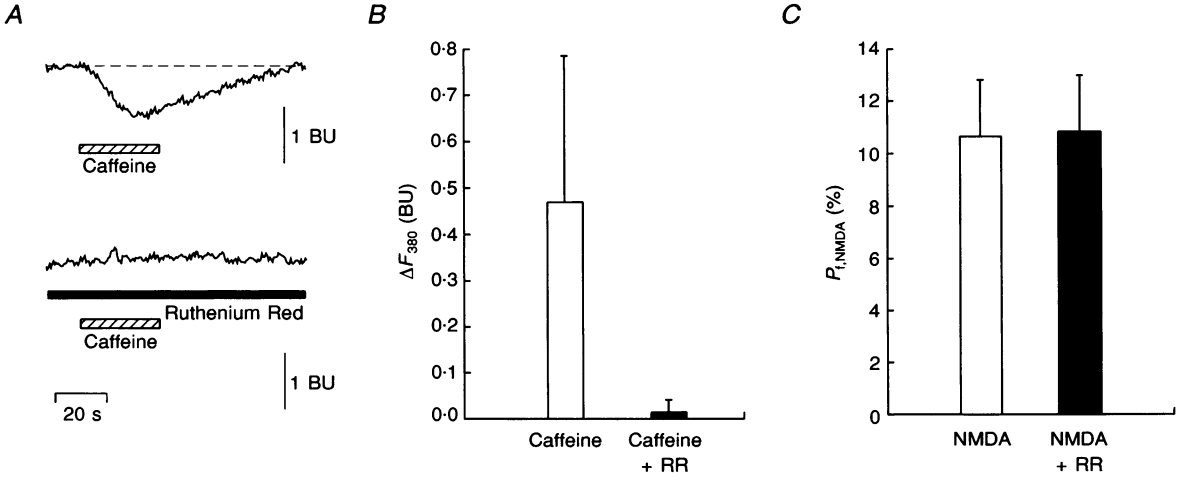

Figure 8. NMDA-mediated Ca^{2+} signals are not contaminated by Ca^{2+} released from ryanodine-sensitive intracellular stores

A, upper trace, change in F_{380} in response to caffeine application (20 mM, 1 min) reflecting Ca^{2+} release from intracellular stores. The experimental conditions were similar to those used for measuring fractional Ca^{2+} currents. Lower trace, recording from another neurone demonstrating the block of the caffeine-mediated Ca^{2+} release when Ruthenium Red (20 μM) was added to the pipette solution. *B*, caffeine-mediated averaged ΔF_{380} responses obtained in the absence (□, $n = 7$ cells) and the presence of intracellular Ruthenium Red (■, $n = 4$ cells). *C*, similarity of mean fractional Ca^{2+} current values through somatic NMDA receptor channels in control conditions (□, $10{\cdot}69 \pm 2{\cdot}13\%$, $n = 37$ cells) and in the presence of intracellular Ruthenium Red (■, $10{\cdot}87 \pm 2{\cdot}14\%$, $n = 6$ cells).

the apical dendrite of a CA1 pyramidal neurone. Current responses of more than 500 pA were required to resolve significant changes in fluorescence in agreement with a low Ca^{2+} permeability of the kainate-gated receptor channels. To avoid possible errors arising from the relatively low signal-to-noise ratio of the fluorescence signals, fractional Ca^{2+} currents were calculated by using the fitting procedure (Fig. 9*B*, see also Methods). The fractional current obtained for dendritic kainate-activated receptor channels of the cell analysed in Fig. 9 was $0{\cdot}5 \pm 0{\cdot}1\%$ ($n = 8$ consecutive applications). The mean fractional Ca^{2+} current through kainate-activated dendritic receptors calculated for all seven neurones tested was $0{\cdot}61 \pm 0{\cdot}16\%$. Similar experiments were performed also for somatic receptor channels (not shown) yielding a mean fractional Ca^{2+} current of $0{\cdot}68 \pm 0{\cdot}20\%$ ($n = 12$ cells).

Figure 10*A* shows the F_{380} changes in response to local dendritic AMPA applications. The fluorescence signals obtained in response to AMPA applications were very similar to those detected with kainate applications. On average, we measured a fractional Ca^{2+} current of $0{\cdot}66 \pm 0{\cdot}25\%$ ($n = 5$ cells) for dendritic and $0{\cdot}58 \pm 0{\cdot}34\%$ ($n = 9$ cells) for somatic AMPA applications.

To compare the Ca^{2+} permeability of the somatic and dendritic AMPA and kainate receptor channels we measured fractional Ca^{2+} currents pairwise from soma and dendrites of the same CA1 neurone. The results of these experiments are shown in Fig. 10*B*. The histogram represents normalized P_f values obtained from four different pairs of somatic and dendritic AMPA and five pairs of somatic and dendritic kainate applications, respectively. These results did not reveal a significant difference between the somatic and dendritic measurements of fractional Ca^{2+} currents. Since kainate is known to activate both AMPA and kainate receptor channels, but AMPA prefers AMPA receptor channels (Lerma, Paternain, Naranjo & Mellström, 1993), our results clearly establish the fractional Ca^{2+} currents of AMPA receptor channels but do not give a conclusive estimate of the Ca^{2+} permeability of kainate receptor channels.

Single-cell RT-PCR analysis of NMDA and AMPA receptor channels

To establish possible molecular correlates of the fractional Ca^{2+} currents measured above, we performed single-cell RT-PCR analyses of AMPA and NMDA receptor mRNAs. In a separate set of experiments the intracellular content of visually identified CA1 pyramidal neurones was harvested and examined for the presence of AMPA and NMDA receptor encoding mRNAs. We used a set of primers specific for GluR-A, GluR-B, GluR-C, GluR-D receptor subunit cDNAs and a set of primers specific for NR2A, NR2B, NR2C receptor subunit cDNAs (see Methods). After the reverse transcriptase reaction was completed, the content of each cell was divided into two parts and the

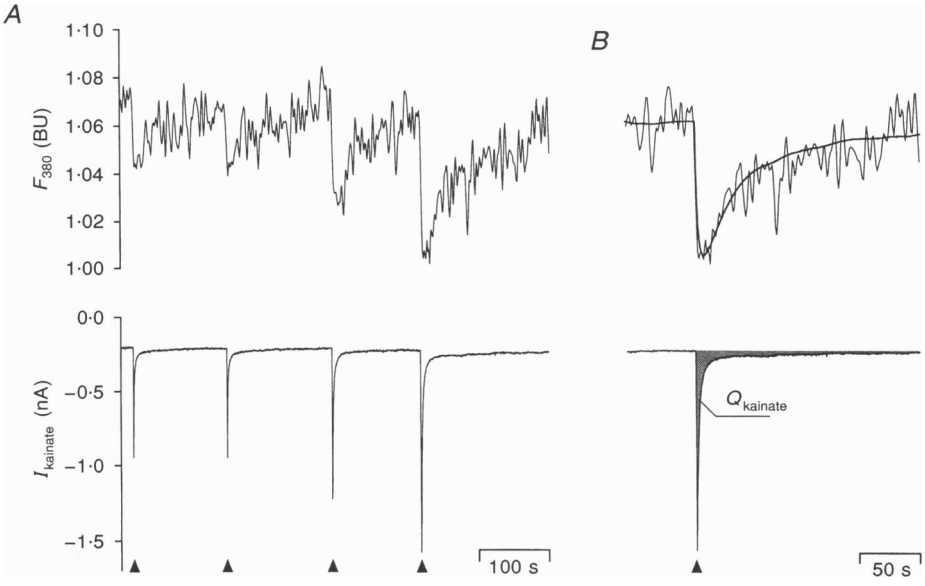

Figure 9. Kainate-mediated dendritic Ca^{2+} entry in a CA1 pyramidal neurone

A, changes in F_{380} (top) and the corresponding whole-cell current responses (bottom) during dendritic kainate applications. *B*, the F_{380} and corresponding whole-cell current response during the last application of kainate on panel *A* shown on an expanded time scale. The superimposed continuous line (top) represents the simulation of the F_{380} response done as explained in the legend of Fig. 2*A*. The shaded area (bottom) represents the total charge ($Q_{kainate}$) that entered in response to the kainate application. A $P_{f,kainate}$ value of 0·51 % was obtained for this particular dendritic kainate application.

Table 1. AMPA and NMDA receptor subunits detected with the single-cell RT-PCR approach

Cell number	AMPA receptor subunits				NMDA receptor subunits		
	GluR-A	GluR-B	GluR-C	GluR-D	NR2A	NR2B	NR2C
Cell 1	+	+	+	−	+	+	−
Cell 2	+	+	+	−	+	+	−
Cell 3	+	+	+	+	+	+	−
Cell 4	+	+	+	−	+	+	−
Cell 5	+	+	−	−	−	+	−
Cell 6	+	+	+	−	+	+	−
Cell 7	+	+	+	−	+	+	−
Cell 8	+	+	+	−	−	+	−
Cell 9	+	+	+	−	+	+	−

Data obtained from 9 visually identified CA1 pyramidal neurones in hippocampal slices of 10- to 15-day-old rats.

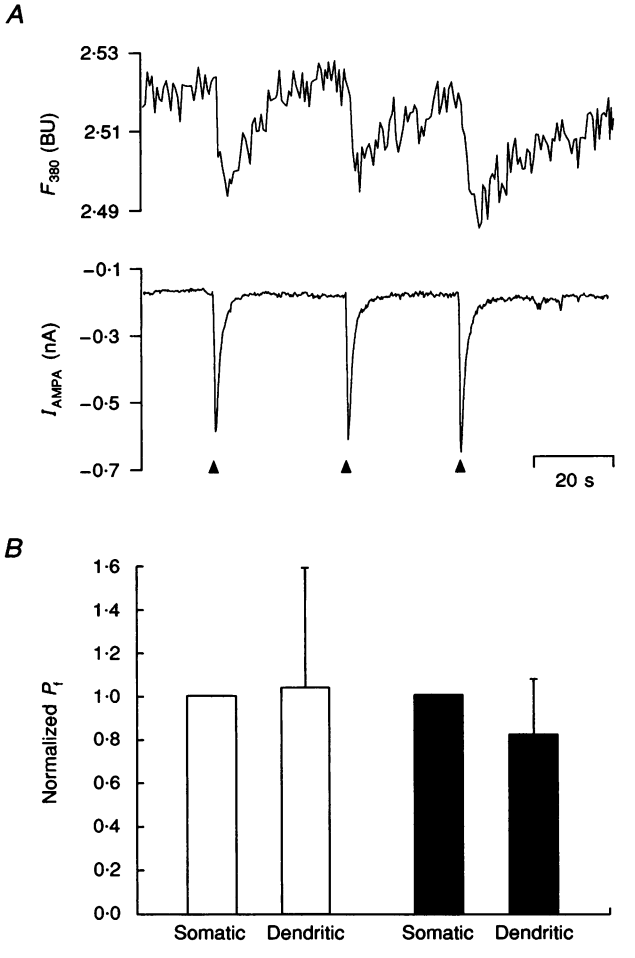

Figure 10. The fractional Ca^{2+} current through non-NMDA receptor channels in somata and dendrites of CA1 pyramidal neurones

A, changes in F_{380} and the corresponding whole-cell current responses during dendritic AMPA applications. The averaged dendritic $P_{f,AMPA}$ value obtained for this cell was $0{\cdot}54 \pm 0{\cdot}16\%$ ($n = 7$ consecutive responses). *B*, similarity of the fractional Ca^{2+} current values measured pairwise during AMPA (□) and kainate (■) applications to somata and dendrites of CA1 pyramidal neurones, respectively ($n = 4$ for AMPA, $n = 5$ for kainate). P_f values for dendritic receptor channels were normalized for each cell with respect to those obtained for the corresponding somatic recordings.

PCR amplification with the AMPA subunit in parallel with the NMDA subunit specific set of primers (see Methods) was performed. All amplified DNAs were analysed with specific restriction enzymes (see Methods).

The results of these experiments are summarized in Table. 1. Out of nine cells tested all expressed GluR-A-, GluR-B- and NR2B-specific mRNAs. All but one neurone contained GluR-C transcripts and only two were lacking NR-2A-encoding mRNA. Altogether we have analysed twenty-three cells for the presence of NMDA receptor specific mRNAs. NR2A- and NR2B-specific mRNAs were found in the majority of cells tested. All cells expressed NR2B-encoding mRNAs, two were lacking NR2A-encoding mRNAs and two contained NR2A-, NR2B- and NR2C-encoding mRNAs. We have not analysed expression of NR1-encoding mRNA, known to be abundantly expressed in hippocampus and throughout all brain structures (see, for example, Monyer, Burnashev, Laurie, Sakmann & Seeburg, 1994).

DISCUSSION

In the present study we used a flux measurement approach to study Ca^{2+} fluxes through somatic and dendritic ionotropic glutamate receptors. While the somatic receptors are almost completely extrasynaptic, the dendritic ones are likely to include a considerable proportion of synaptic receptors. Our measurements establish the fraction of Ca^{2+} flowing through these cation channels and provide evidence that CA1 pyramidal neurones express in soma and dendrites functionally similar NMDA and non-NMDA receptor channels. We also report the expression pattern of NMDA and AMPA receptor subunits of these neurones obtained under similar experimental conditions using the single-cell RT-PCR method.

Methodological considerations concerning the measurement of the dendritic transmembrane Ca^{2+} fluxes

In the present study the flux measurement approach developed by Neher & Augustine (1992) and Schneggenburger *et al.* (1993) was used to study Ca^{2+} fluxes in the cells with a developed dendritic tree. The following precautions were taken in order to measure correctly ionic currents: (1) voltage-gated conductances were effectively blocked (see Methods); (2) only agonist-induced currents with the smallest possible amplitudes were included in the analyses; (3) the series resistance was always compensated; and (4) dendritic recordings were obtained from proximal sites of less than 100 μm distance from the soma. Thus, we estimated that even for the least favourable cases the voltage-clamp error was less than 10% . This estimate is well supported by the results of Hestrin, Nicoll, Perkel & Sah (1990) who analysed the voltage control in whole-cell experiments in pyramidal neurones from adult rats.

The main source of a possible error when measuring transmembrane Ca^{2+} fluxes appeared to be an incorrect estimate of the fluorescence change. By placing the ionophoresis pipette sufficiently close to the dendrites of interest and by applying agonist for a short time (20–50 ms), Ca^{2+}-dependent changes in fluorescence were restricted to a relatively small region (Figs 5*Ab* and 6). Thus, it was possible to avoid a significant activation of receptors located on dendrites that were not in the plane of focus. Under these experimental conditions, measured P_f values remained constant over a wide range of the amplitudes of evoked ionic currents (Figs 6, 7, 9 and 10). However, P_f values fell dramatically when the area of the fluorescence measurement was smaller than the area where ionic currents were activated or when the buffer capacity of fura-2 was insufficient to buffer all incoming Ca^{2+} (for example with a large increase in basal $[Ca^{2+}]_i$).

Because the coefficient f_{max} was used to estimate the change in Ca^{2+}-sensitive fluorescence signal per unit of entering Ca^{2+} charge (see Methods), the precise estimation of this value was important and affected all results obtained in the present study. Although f_{max} was estimated in this study with three different techniques (see Methods), for safety we compared this value with the f_{max} value obtained for 3- to 5-day-old cerebellar Purkinje neurones using the same experimental set-up. At this stage of development, Purkinje neurones do not have large dendritic processes so they can be electrically clamped well and loss of fluorescence from tiny dendritic arborizations is negligible. In this preparation, the f_{max} value was found to be 8·4 BU nC^{-1} (Tempia *et al.* 1996) similar to the values obtained in our study. Very similar f_{max} values were also found in other studies (Schneggenburger *et al.* 1993; Zhou & Neher, 1993; Burnashev *et al.* 1995) that have used the same 'standard' fluorescent beads. Taken together these data demonstrate, that when using the same fluorescence 'standard' and a highly selective source of Ca^{2+} entry, f_{max} becomes independent of the experimental set-up. On the other hand, it indicates that under our experimental conditions in cells with a developed dendritic tree, the f_{max} value was measured correctly, although loss of fluorescence signal from tiny dendrites, which are out of focus, cannot be entirely excluded.

Fractional Ca^{2+} current through NMDA receptor channels

For the NMDA receptor channels on the somata and dendrites of CA1 pyramidal neurones in hippocampal slices we found P_f values of 10·69 and 10·70% respectively. In standard external saline, NMDA-activated ionic currents showed their characteristic behaviour with a region of negative slope conductance within the range of holding potentials from −70 to −20 mV, and a peak amplitude at −20 mV (see Fig. 3), thus resembling the properties of synaptic NMDA receptor channels reported previously

(Hestrin *et al.* 1990; Keller, Konnerth & Yaari, 1991). The fractional Ca^{2+} current through NMDA receptor channels was not dependent on the presence of extracellular Mg^{2+} and was constant over a wide range of holding potentials (Fig. 4). The voltage dependence of P_f was well described by the prediction of the GHK current equation. For recombinant NMDA receptors, Burnashev *et al.* (1995) obtained similar results concerning the voltage dependence of P_f but found that the calcium dependence of P_f is not well described by the GHK current equation (Fig. 4; Burnashev *et al.* 1995).

To compare our results with data reported by others we have calculated P_{Ca}/P_M from our measured P_f values (using eqn (5), see Methods). For the experimental conditions used in this study (e.g. 1·6 mM Ca^{2+}, 155 mM monovalents outside, 136·2 mM monovalents inside, $V_h = -60$ mV) the value of P_{Ca}/P_M is 2·91 for both somatic and dendritic NMDA receptor channels. Using reversal potential measurements, Spruston, Jonas & Sakmann (1995) obtained a P_{Ca}/P_{Cs} value of 3·6 for NMDA receptor channels on dendrites of CA1 neurones in a similar hippocampal slice preparation, while Mayer & Westbrook (1987) and Iino *et al.* (1990) obtained values of P_{Ca}/P_M of 4·03 and 6·2, respectively, for somatic NMDA receptors in cultured hippocampal neurones. Note the scatter of the P_{Ca}/P_M values estimated, under GHK assumptions, from reversal potential measurements in ion substitution experiments. Interestingly, a much closer similarity was found for the P_f values that were directly measured either in cultured hippocampal neurones (10%, 2 mM $[Ca^{2+}]_o$, Jahr & Stevens, 1993; 12·4%, 2·5 mM $[Ca^{2+}]_o$, Rogers & Dani, 1995) or in CA1 pyramidal neurones of hippocampal slices (10·7%, 1·6 mM $[Ca^{2+}]_o$, present study).

Fractional Ca^{2+} current through non-NMDA receptor channels

Ionophoretic applications of AMPA or kainate to CA1 hippocampal pyramidal neurones resulted in a small amount of Ca^{2+} entry, consistent with an earlier report by Jonas & Sakmann (1992) showing that these neurones express non-NMDA receptors with low Ca^{2+} permeability. Nevertheless, we were able to measure the fractional Ca^{2+} current through these receptor channels. We obtained P_f values of 0·58% for somatic AMPA applications and 0·68% for somatic kainate applications.

In the present study we did not aim to identify kainate-selective glutamate receptors. But because this receptor type was found to be expressed in cultured hippocampal neurones (Lerma *et al.* 1993) we have separated our data obtained from AMPA and kainate applications. In fact, we found slightly, but not significantly, lower P_f values for AMPA than for kainate-activated receptor channels.

Similar Ca^{2+} permeability of the somatic and dendritic glutamate receptor channels

In the present study we established the fractional Ca^{2+} currents through dendritic glutamate receptor channels. For the NMDA-, AMPA- and kainate-activated receptor channels situated on the apical dendrites we have found P_f values of 10·7, 0·66 and 0·61%, respectively. These values were not significantly different from the somatic P_f values (Figs 7 and 10). This finding contrasts with results obtained by Lerma, Morales, Ibarz & Somohano (1994) for acutely dissociated hippocampal neurones. Measuring the degree of rectification of the I–V relationships for kainate-induced whole-cell currents these authors came to the conclusion that Ca^{2+}-permeable AMPA receptors are preferentially located in the dendritic tree of hippocampal neurones (Lerma *et al.* 1994). Conversely, Spruston *et al.* (1995) found similar Ca^{2+} permeabilities for somatic and dendritic AMPA- and NMDA receptor channels when analysing outside-out membrane patches isolated from the soma or the apical dendrites of CA1 and CA3 pyramidal neurones in rat hippocampal slices. It is worth noting here that in the present study, as well as in all studies cited here, the properties of the rather proximal apical dendrites have been studied. Therefore, it cannot entirely be excluded that glutamate receptors with different properties may be situated on the dendritic spines. On the other hand, immunocytochemical studies (Craig, Blackstone, Huganir & Banker, 1993) have suggested that synaptic and extrasynaptic glutamate receptors have the same subunit composition.

Molecular basis for the Ca^{2+} permeability of glutamate receptor channels in CA1 hippocampal pyramidal neurones.

Based on the study of recombinant glutamate receptors, the functional characteristics and Ca^{2+} permeability for some types of homomeric and heteromeric glutamate receptors expressed in human embryonic kidney cells (HEK 293 cells; Monyer *et al.* 1994; Burnashev *et al.* 1995) have been reported recently. However, this data may not directly apply to neuronal cells as they appear to co-express a great variety of different glutamate receptor subunits (Lambolez *et al.* 1992; Bochet *et al.* 1994; Jonas *et al.* 1994; Monyer *et al.* 1994).

For CA1 pyramidal hippocampal neurones, we found that the GluR-A, GluR-B and GluR-C AMPA receptor subunits and the NR2A and NR2B NMDA receptor subunits were co-expressed in the same cell. It is widely accepted that the specific properties of functionally different NMDA receptor subtypes are imparted on the heteromeric receptor channel by the particular NR2 subunit, while NR1 receptors are abundantly expressed throughout the brain (Moriyoshi, Masu, Ishii, Shigemoto, Mizuno & Nakanishi, 1991; Monyer *et al.* 1992, 1994). Therefore, we have restricted our

analyses to the NR2A, NR2B and NR2C NMDA receptor subunits (the NR2D subunit was found not to be expressed in significant amounts in the hippocampus (Monyer *et al.* 1994)). We have found that two different NR2 receptor subunits, namely NR2A and NR2B are abundantly expressed in hippocampal CA1 pyramidal neurones, as was implicitly suggested from an *in situ* hybridization study (Monyer *et al.* 1994). This molecular evidence is in agreement with functional properties of the NMDA receptor channels studied here (e.g. the strength of the Mg^{2+} block) that resemble the properties of NR1–NR2A and NR1–NR2B recombinant NMDA receptors (Monyer *et al.* 1994). Most notably, the P_f values established in our study for somatic and dendritic NMDA receptor channels (10·7%) are in striking agreement with the value obtained by Burnashev *et al.* (1995) for the recombinant NR1–NR2A receptor channels (11%).

We have also found that the GluR-B subunit, known to control the Ca^{2+} permeability through AMPA receptor channels (Hume *et al.* 1991; Burnashev *et al.* 1992), is abundantly expressed in CA1 hippocampal pyramidal neurones. This finding is in a good agreement with the measured low fractional Ca^{2+} current through AMPA-activated receptor channels. Although we have not discriminated between edited and unedited forms of GluR-B in this study, there is good reason to assume that all GluR-B detected here is in the edited form regarding data obtained by PCR analysis of rat brain RNAs (Burnashev *et al.* 1992). These authors have reported that the unedited form of the GluR-B subunit did not exceed 1% in early (embryonic day 14 (E14)–postnatal day 0 (P0) and 0·01% in later (P8) developmental stages. In the neocortex of 12- to 16-day-old rats the unedited form of GluR-B subunit was never found either in interneurones or in pyramidal cells (Jonas *et al.* 1994). In addition, the fractional Ca^{2+} current reported here is very close to that obtained by Burnashev and co-workers for recombinant AMPA receptor channels when GluR-A and GluR-B (edited form) subunits were co-expressed together in HEK 293 cells.

The hypothesis that AMPA receptor subunits co-expressed in CA1 pyramidal neurones form heteromeric receptor complexes containing the edited GluR-B subunit, is supported by the observations based on measured P_f values as well as on analyses of pseudocolour fluorescence images recorded during AMPA or kainate applications (similar to shown in Fig. 5 for NMDA application). We have never obtained a P_f value higher than 0·9% in response to dendritic or somatic AMPA or kainate applications and have never seen any 'hot spots' on the pseudocolour image that would correspond to receptors with a high Ca^{2+} permeability. These findings are in agreement with immunocytochemical data obtained recently on cultured rat hippocampal neurones (Craig *et al.* 1993). Using antibodies raised against GluR-A and GluR-B–GluR-C subunits a complete colocalization of these AMPA-selective glutamate receptor subunits on the somata, dendrites and dendritic spines of hippocampal pyramidal-shaped neurones was observed.

In conclusion, we have determined here the Ca^{2+} permeability for dendritic and somatic ionotropic glutamate receptors by using a fluorometric flux measurement approach. The previously reported finding that, in cultured pyramidal hippocampal neurones, glutamate receptors with the same subunit composition are found on dendritic spines (Craig *et al.* 1993) allows the assumption that synaptic AMPA receptors have similar Ca^{2+} permeability as that reported here for the extrasynaptic somatic and subsynaptic dendritic AMPA receptor channels. However, additional experiments are required to test whether the Ca^{2+} permeability of synaptic receptor channels is identical to that found here in the dendritic recordings. It seems that the flux measurement approach is a useful method to solve this problem.

Alford, S., Frenguelli, B. G., Schofield, J. G. & Collingridge, G. L. (1993). Characterization of Ca^{2+} signals induced in hippocampal CA1 neurones by the synaptic activation of NMDA receptors. *Journal of Physiology* **469**, 693–716.

Audinant, E., Lambolez, B., Rossier, J. & Crepel, F. (1994). Activity-dependent regulation of *N*-methyl-D-aspartate receptor subunit expression in rat cerebellar granule cells. *European Journal of Neuroscience* **6**, 1792–1800.

Bliss, T. V. P. & Collingridge, G. L. (1993). A synaptic model of memory: long-term potentiation in the hippocampus. *Nature* **361**, 31–39.

Bochet, P., Audinat, E., Lambolez, B., Crepel, F., Rossier, J., Iino, M., Tsuzuki, K. & Ozawa, S. (1994). Subunit composition at the single-cell level explains functional properties of a glutamate-gated channel. *Neuron* **12**, 383–388.

Burnashev, N., Monyer, H., Seeburg, P. H. & Sakmann, B. (1992). Divalent ion permeability of AMPA receptor channels is dominated by the edited form of a single subunit. *Neuron* **8**, 189–198.

Burnashev, N., Zhou, Z., Neher, E. & Sakmann, B. (1995). Fractional calcium currents through recombinant GluR channels of the NMDA, AMPA and kainate receptor subtypes. *Journal of Physiology* **485**, 403–418.

Craig, A. M., Blackstone, C. D., Huganir, R. L. & Banker, G. (1993). The distribution of glutamate receptors in cultured rat hippocampal neurons: postsynaptic clustering of AMPA-selective subunits. *Neuron* **10**, 1055–1068.

Edwards, F. A., Konnerth, A., Sakmann, B. & Takahashi, T. (1989). A thin slice preparation for patch-clamp recordings from neurones of the mammalian central nervous system. *Pflügers Archiv* **414**, 600–612.

Eilers, J., Schneggenburger, R. & Konnerth, A. (1995). Patch clamp and calcium imaging in brain slices. In *Single Channel Recording*, ed. Sakmann, B. & Neher, E., pp. 213–229. Plenum Publishing Co., New York.

GRYNKIEWICZ, G., POENIE, M. & TSIEN, R. Y. (1985). A new generation of Ca^{2+} indicators with greatly improved fluorescent properties. *Journal of Biological Chemistry* **260**, 3440–3450.

HESTRIN, S., NICOLL, R. A., PERKEL, D. J. & SAH, P. (1990). Analysis of excitatory synaptic action in pyramidal cells using whole-cell recordings from rat hippocampal slices. *Journal of Physiology* **422**, 203–225.

HOLLMANN, M. & HEINEMANN, S. (1994). Cloned glutamate receptors. *Annual Review of Neuroscience* **17**, 31–108.

HOLLMANN, M., MARON, C. & HEINEMANN, S. (1994). *N*-glycosylation site tagging suggests a three transmembrane domain topology for the glutamate receptor GluR1. *Neuron* **13**, 1331–1343.

HUME, R. I., DINGLEDINE, R. & HEINEMANN, S. F. (1991). Identification of a site in glutamate receptor subunits that controls calcium permeability. *Science* **253**, 1028–1031.

IINO, M., OZAWA, S. & TSUZUKI, K. (1990). Permeation of calcium through excitatory amino acid receptor channels in cultured rat hippocampal neurones. *Journal of Physiology* **424**, 151–165.

JAHR, G. E. & STEVENS, C. F. (1993). Calcium permeability of the *N*-methyl-D-aspartate receptor channel in hippocampal neurons in culture. *Proceedings of the National Academy of Sciences of the USA* **90**, 11573–11577.

JONAS, P., RACCA, C., SAKMANN, B., SEEBURG, P. H. & MONYER, H. (1994). Differences in Ca^{2+} permeability of AMPA-type glutamate receptor channels in neocortical neurons caused by differential GluR-B subunit expression. *Neuron* **12**, 1281–1289.

JONAS, P. & SAKMANN, B. (1992). Glutamate receptor channels in isolated patches from CA1 and CA3 pyramidal cells of rat hippocampal slices. *Journal of Physiology* **455**, 143–171.

KANO, M., GARASCHUK, O., VERKHRATSKY, A. & KONNERTH, A. (1995). Ryanodine receptor-mediated intracellular calcium release in rat cerebellar Purkinje neurones. *Journal of Physiology* **487**, 1–16.

KELLER, B. U., HOLLMANN, M., HEINEMANN, S. & KONNERTH, A. (1992). Calcium influx through subunits GluR1/GluR3 of kainate/AMPA receptor channels is regulated by cAMP dependent protein kinase. *EMBO Journal* **11**, 891–896.

KELLER, B. U., KONNERTH, A. & YAARI, Y. (1991). Patch clamp analysis of excitatory synaptic currents in granule cells of rat hippocampus. *Journal of Physiology* **435**, 275–293.

LAMBOLEZ, B., AUDINAT, E., BOCHET, P., CREPEL, F. & ROSSIER, J. (1992). AMPA receptor subunits expressed by single Purkinje cells. *Neuron* **9**, 247–258.

LERMA, J., MORALES, M., IBARZ, J. M. & SOMOHANO, F. (1994). Rectification properties and Ca^{2+} permeability of glutamate receptor channels in hippocampal cells. *European Journal of Neuroscience* **6**, 1080–1088.

LERMA, J., PATERNAIN, A. V., NARANJO, J. R. & MELLSTRÖM, B. (1993). Functional kainate-selective glutamate receptors in cultured hippocampal neurons. *Proceedings of the National Academy of Sciences of the USA* **90**, 11688–11692.

LIPTON, S. A. (1993). Prospects for clinically tolerated NMDA antagonists: open channel blockers and alternative redox states of nitric oxide. *Trends in Neurosciences* **16**, 527–532.

MALENKA, R. & NICOLL, R. (1993). NMDA-receptor-dependent synaptic plasticity: multiple forms and mechanisms. *Trends in Neurosciences* **16**, 521–526.

MAYER, M. & WESTBROOK, G. L. (1987). Permeation and block of *N*-methyl-D-aspartic acid receptor channels by divalent cations in mouse cultured central neurones. *Journal of Physiology* **394**, 501–527.

MONYER, H., BURNASHEV, N., LAURIE, D. J., SAKMANN, B. & SEEBURG, P. H. (1994). Developmental and regional expression in the rat brain and functional properties of four NMDA receptors. *Neuron* **12**, 529–540.

MONYER, H., SPRENGEL, R., SCHOEPFER, R., HERB, A., HIGUCHI, M., LOMELI, H., BURNASHEV, N., SAKMANN, B. & SEEBURG, P. H. (1992). Heteromeric NMDA receptors: Molecular and functional distinction of subtypes. *Science* **256**, 1217–1221.

MORIYOSHI, K., MASU, M., ISHII, T., SHIGEMOTO, R., MIZUNO, N. & NAKANISHI, S. (1991). Molecular cloning and characterization of the rat NMDA receptor. *Nature* **354**, 31–37.

NEHER, E. (1989). Combined fura-2 and patch clamp measurements in rat perioneal mast cells. In *Neuromuscular Junction*, ed. SELLIN, L., LIBELIUS, R. & THESLEFF, S., pp. 65–76. Elsevier, Amsterdam.

NEHER, E. & AUGUSTINE, G. J. (1992). Calcium gradients and buffers in bovine chromaffin cells. *Journal of Physiology* **450**, 273–301.

NOWAK, L., BREGESTOVSKI, P., ASCHER, P., HERBET, A. & PROCHIANTZ, A. (1984). Magnesium gates glutamate-activated channels in mouse central neurones. *Nature* **307**, 462–465.

ROGERS, M. & DANI, J. A. (1995). Comparison of quantitative calcium flux through NMDA, ATP, ACh receptor channels. *Biophysical Journal* **68**, 501–506.

SCHNEGGENBURGER, R., ZHOU, Z., KONNERTH, A. & NEHER, E. (1993). Fractional contribution of calcium to the cation current through glutamate receptor channels. *Neuron* **11**, 133–143.

SOMMER, B., KÖHLER, M., SPRENGEL, R. & SEEBURG, P. H. (1991). RNA editing in brain controls a determinant of ion flow in glutamate-gated channels. *Cell* **67**, 11–19.

SPRUSTON, N., JONAS, P. & SAKMANN, B. (1995). Dendritic glutamate receptor channels in rat hippocampal CA3 and CA1 pyramidal neurons. *Journal of Physiology* **482**, 325–352.

TEMPIA, F., KANO, M., SCHNEGGENBURGER, R., SCHIRRA, C., GARASCHUK, O., PLANT, T. & KONNERTH, A. (1996). Fractional calcium current through neuronal AMPA-receptor channels with a low calcium permeability. *Journal of Neuroscience* **16**, 456–466.

WISDEN, W. & SEEBURG, P. H. (1993). Mammalian ionotropic glutamate receptors. *Current Opinions in Neurobiology* **3**, 291–298.

ZHOU, Z. & NEHER, E. (1993). Calcium permeability of nicotinic acetylcholine receptor channels in bovine adrenal chromaffin cells. *Pflügers Archiv* **425**, 511–517.

Acknowledgements

The authors thank Dr T. D. Plant for comments on the manuscript and Nicole Wilhelm for excellent technical assistance. This work was supported by grants from the DFG (SFB 246), the BMFB and INTAS (94-4072).

Authors' present addresses

R. Schneggenburger: Laboratoire de Neurobiologie, Ecole Normale Supérieure, 46 rue d'Ulm, 75005 Paris, France.

F. Tempia: Department of Human Anatomy and Physiology, Corso Raffaelo 30, 10125 Torino, Italy.

Received 12 June 1995; accepted 3 October 1995.